



UNIVERSITY OF LEEDS

This is a repository copy of *Breaking Isolation to Form New Networks: pH-Triggered Changes in Connectivity Inside Lipid Nanoparticles*.

White Rose Research Online URL for this paper:

<https://eprints.whiterose.ac.uk/179053/>

Version: Supplemental Material

Article:

Xu, Z, Seddon, JM, Beales, P orcid.org/0000-0001-9076-9793 et al. (2 more authors)
(2021) *Breaking Isolation to Form New Networks: pH-Triggered Changes in Connectivity Inside Lipid Nanoparticles*. Journal of the American Chemical Society. ISSN 0002-7863

<https://doi.org/10.1021/jacs.1c06244>

© 2021 American Chemical Society. This is an author produced version of an article published in Journal of the American Chemical Society (JACS). Uploaded in accordance with the publisher's self-archiving policy.

Reuse

Items deposited in White Rose Research Online are protected by copyright, with all rights reserved unless indicated otherwise. They may be downloaded and/or printed for private study, or other acts as permitted by national copyright laws. The publisher or other rights holders may allow further reproduction and re-use of the full text version. This is indicated by the licence information on the White Rose Research Online record for the item.

Takedown

If you consider content in White Rose Research Online to be in breach of UK law, please notify us by emailing eprints@whiterose.ac.uk including the URL of the record and the reason for the withdrawal request.



eprints@whiterose.ac.uk
<https://eprints.whiterose.ac.uk/>

Supporting Information

Breaking isolation to form new networks: pH-triggered changes in connectivity inside lipid nanoparticles

Zexi Xu^{1,3}, John M. Seddon², Paul A. Beales³, Michael Rappolt¹ and Arwen I.I. Tyler^{1*}

¹ School of Food Science and Nutrition, University of Leeds, Leeds, LS2 9JT, United Kingdom.

² Department of Chemistry, Imperial College London, London W12 0BZ, United Kingdom.

³ School of Chemistry and Astbury Centre for Structural Molecular Biology, University of Leeds, United Kingdom.

Corresponding Author

* Email: A.I.I.Tyler@leeds.ac.uk

Supporting information Section 1: Estimation of micellosome and hexosome size ratios

Knowing the lattice parameters, a , for the underlying Fd3m and H_{II} phase of the micellosomes and hexosomes, respectively, and making an estimation of the position of the Gibbs-dividing surface (this concerns the effective lipid length l), it is straight forward to calculate water radii (R_W) and water volume fractions (Φ_W) of each respective phase.¹⁻² These parameters are summarized in the following equations for the water radii of the small (S) and big (B) micelles in the Fd3m phase as well as for the water radius in the H_{II} phase (S1-S3). The water volume fractions are given in S4 and S5:

$$R_W(S) = \sqrt{2}/8 - l \quad (S1)$$

$$R_W(B) = \sqrt{3}/8 - l \quad (S2)$$

$$R_W(H_{II}) = a/2 - l \quad (S3)$$

$$\Phi_W(\text{Fd3m}) = (16 \cdot 4\pi/3 R_W(S)^3 + 8 \cdot 4\pi/3 R_W(B)^3)/a^3 \quad (S4)$$

$$\Phi_W(H_{II}) = \pi R_W(H_{II})^2/(\sqrt{3}/2 a^2) \quad (S5)$$

Finally, we can estimate the ratio of particle diameters of the micellosomes and hexosomes, $D(H_{II})/D(\text{Fd3m})$. Under the assumption that (i) both particles are approximately spherical in shape, and (ii) the entire volume change of the particle is due to changes in the water volume, V_W , i.e., assuming the lipid volume, V_L , to be unaltered during a micellosome to hexosome transition, and using the experimental values of $a_{H_{II}} = 47 \text{ \AA}$, $a_{\text{Fd3m}} = 149 \text{ \AA}$ and varying l from 13 to 18 \AA , we obtain particle size increases to vary from 0.6 to 2%. Note the ratio of $V_{\text{Fd3m}}/V_{H_{II}}$ equals $1 - \Delta\Phi_W$.

Supporting information Section 2: Lattice parameter analysis from Cryo-TEM data

The lattice parameter of the corresponding individual nanoparticle were determined by the positions of the detected peaks in the FFT, which correspond to the reflections from the planes defined by their Miller indices ($h k l$). The lattice parameter is determined as follows:

$$a = d_{hkl} \cdot (h^2 + k^2 + l^2) \quad (S6)$$

where d_{hkl} is the d-spacing of the plane (hkl) which can be measured using Fiji.³ The d -spacing of each reflection in the FFT was determined using TrackMate⁴ and so the lattice parameter of the individual nanoparticle can be calculated. The indexing of the data can be shown as a plot of the reciprocal d -spacing versus $\sqrt{(h^2 + k^2 + l^2)}$. For a correctly indexed cubic structure,

such a plot should be linear with a gradient equal to the reciprocal of the lattice parameter of the Fd3m phase and should pass through the origin.⁵

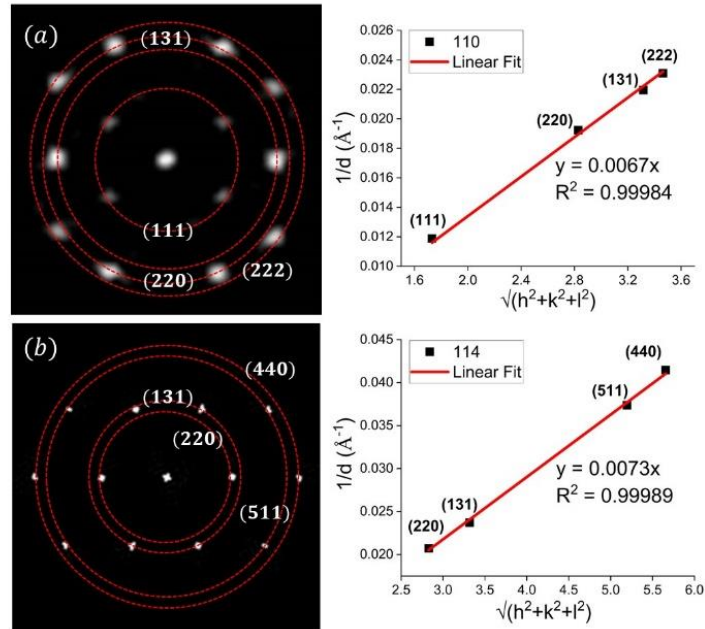


Figure S1: Indexing of FFT reflections to obtain the lattice parameter of Fd3m micellosomes. (a) Left: FFT generated from the cryo-TEM image in Figure 4a. The 111, 220, 131 and 222 reflections were indexed. Right: The observed reciprocal spacings versus $\sqrt{h^2+k^2+l^2}$ for the Fd3m nanoparticle in Figure 4a and the fitting (red line) to a linear plot through the origin confirms the structure has been correctly indexed to the Fd3m space group with a lattice parameter of 149.3 Å. (b) Left: FFT generated from the cryo-TEM image in Figure 4e where the 220, 131, 511 and 440 reflections were observed. Right: fit of the reciprocal spacings versus $\sqrt{h^2+k^2+l^2}$ confirm the indexing as space group Fd3m with a lattice parameter of 137 Å.

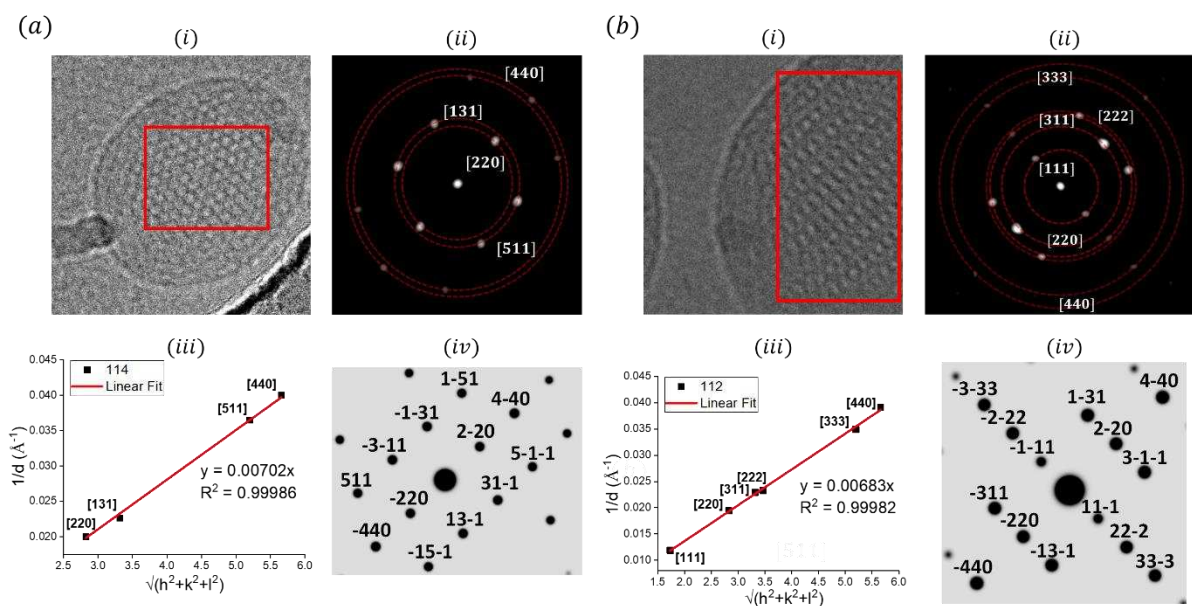


Figure S2: Indexing of FFT reflections of a further two Fd3m micelles of MO:Olalc:DOBAQ 56:41:3 mol% to obtain the lattice parameter. (a) (i) Cryo-TEM image of a nanoparticle aligned along the [114] orientation with respect to the electron beam. The red box indicates the region used to apply the FFT. (a) (ii) FFT generated from the cryo-TEM image in (a) (i) where the 220, 131, 511 and 440 reflections were observed. (a) (iii) Fit of the reciprocal spacings versus $\sqrt{(h^2+k^2+l^2)}$ confirm the indexing as space group Fd3m with a lattice parameter of 142.5 Å. (a) (iv) Simulated transmission electron microscopy (TEM) diffraction pattern viewed down the (114) plane normal of an Fd3m phase with assigned Miller indices. The corresponding FFT applied to the red box region of (a) (i) is in excellent agreement with the simulated pattern. Each theoretical reflection from the simulated diffraction pattern indexed in (a) (iv) corresponds to the same reflection in (a) (ii). (b) (i) Cryo-TEM image of a nanoparticle aligned along the [112] orientation. The red box indicates the region used to apply the FFT. (b) (ii) FFT generated from the cryo-TEM image in (b) (i) where the 111, 220, 311, 222, 333 and 440 reflections were observed. (b) (iii) Fit of the reciprocal spacings versus $\sqrt{(h^2+k^2+l^2)}$ confirm the indexing as space group Fd3m with a lattice parameter of 146.4 Å. (a) (iv) Simulated transmission electron microscopy (TEM) diffraction pattern viewed down the (112) plane normal of an Fd3m phase with assigned Miller indices. The experimental and simulated patterns are in excellent agreement. Each theoretical reflection from the simulated diffraction pattern indexed in (b) (iv) corresponds to the same reflection in (b) (ii).

Supporting Information Section 3: Determination of the micelle positions in Fd3m nanoparticles

Micelle positions and packing in Fd3m nanoparticles were determined by comparing our experimental inverse FFT image extracted from **Figure 4a** (**Figure S3a**, not Gaussian blurred) with the electron density map of a previously published DOPC:DOG 1:2 mol% system (**Figure S3b** and **S3c**) adopting an Fd3m phase. Details on experimental X-ray spacings, intensities,

moduli of the structure factors, phasing and method used to calculate the electron density maps can be found in Tyler *et al.*⁶ Electron density maps were reconstructed for the (110) section (symmetry $c2mm$) through $(5a/8, 5a/8, z)$ as shown in **Figure S3b** and **S3c**. A direction perpendicular to the (110) section was chosen and five 2-D serial sections of the 3-D electron density map, with a distance between each section of $1/(4\sqrt{2})$, revealed the distribution of the different micelles along the (110) section within one period of variation of the electron density map. It should be noted that in certain 2-D sections, the smaller micelles can appear larger than the micelles that are in fact bigger. This occurs if the section cuts through the centers of the smaller micelles and so samples their maximum radius, but is offset from the centers of the larger micelles and so samples a smaller section through their pseudo spherical shape. **Figure S3d** shows the (110) plane in the $Fd\bar{3}m$ unit cell (only the big micelles are shown here). **Figure S3b** shows the electron density map from the plane that cuts through the center of big micelle, from which clear big to big (d_{B-B}), and small to small (d_{S-S}) micellar distances can be observed (note, these are the shortest micelle to micelle distances). In **Figure S3c**, the B^*-B^* micelle distance defines the nearest big to big micelle distance in this particular plane, i.e., the nearest micelle distance, referring to their hexagonal arrangement. The length of B^*-B^* can be calculated as followed:

$$d_{B^*-B^*} = 2 \cdot d_{S-S} \quad (S7)$$

Depending on the 2-D section viewed, some only show the big micelles (**Figure S3c**), which exactly match the pattern from the inverse FFT and correspond to B^*-B^* distances.

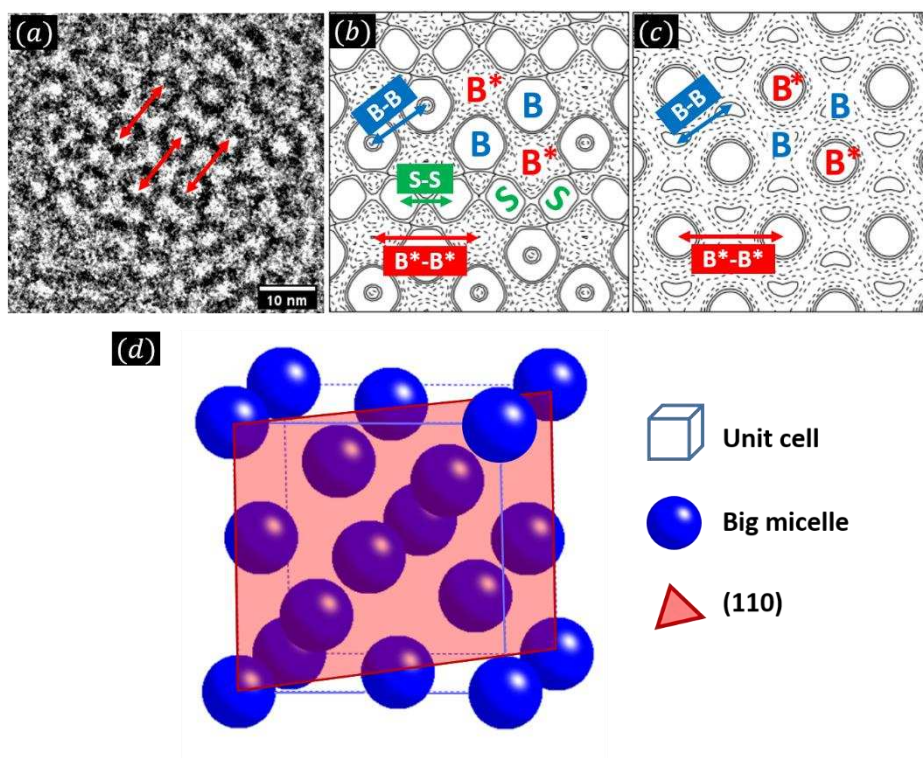


Figure S3: Geometrical details of the (110) plane given in the Fd3m phase. a) Inverted FFT image extract from Figure 4c which has not been image processed; electron density maps of DOPC/DOG 1:2 adopting an Fd3m phase at different heights: b) central cut through the big micelles (adapted from Tyler *et al.* PCCP with permission from the PCCP Owner Societies); c) lower central cut through the big micelles; e) schematic of the Fd3m unit cell with the (110) plane shown in red. Only the big micelles are shown in the schematic.

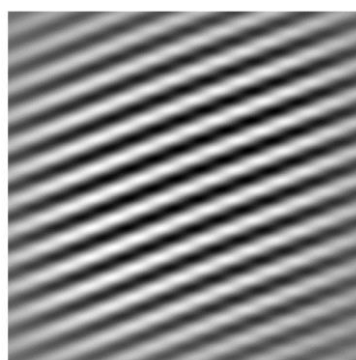


Figure S4: Inverse FFT of only the -220 and 220 reflections (corresponding to $\sqrt{8}$ reflections) from the nanoparticle in Figure 4e, highlighting that the S-S micelle distance in the [114] orientation corresponds to the plane to plane distance of the small micelles rather than the distance between two adjacent small micelles shown in Figure S3b.

References:

1. Rappolt, M.; Hodzic, A.; Sartori, B.; Ollivon, M.; Laggner, P., Conformational and hydrational properties during the L(beta)- to L(alpha)- and L(alpha)- to H(II)-phase transition in phosphatidylethanolamine. *Chem Phys Lipids* **2008**, *154* (1), 46-55.
2. Yagmur, A.; Rappolt, M., Chapter Five - The Micellar Cubic Fd3m Phase: Recent Advances in the Structural Characterization and Potential Applications. In *Advances in Planar Lipid Bilayers and Liposomes*, Iglič, A.; Kulkarni, C. V., Eds. Academic Press: 2013; Vol. 18, pp 111-145.
3. Schindelin, J.; Arganda-Carreras, I.; Frise, E.; Kaynig, V.; Longair, M.; Pietzsch, T.; Preibisch, S.; Rueden, C.; Saalfeld, S.; Schmid, B.; Tinevez, J. Y.; White, D. J.; Hartenstein, V.; Eliceiri, K.; Tomancak, P.; Cardona, A., Fiji: an open-source platform for biological-image analysis. *Nat Methods* **2012**, *9* (7), 676-82.
4. Tinevez, J. Y.; Perry, N.; Schindelin, J.; Hoopes, G. M.; Reynolds, G. D.; Laplantine, E.; Bednarek, S. Y.; Shorte, S. L.; Eliceiri, K. W., TrackMate: An open and extensible platform for single-particle tracking. *Methods* **2017**, *115*, 80-90.
5. Tyler, A. I.; Law, R. V.; Seddon, J. M., X-ray diffraction of lipid model membranes. *Methods Mol Biol* **2015**, *1232*, 199-225.
6. Tyler, A. I.; Shearman, G. C.; Brooks, N. J.; Delacroix, H.; Law, R. V.; Templer, R. H.; Ces, O.; Seddon, J. M., Hydrostatic pressure effects on a hydrated lipid inverse micellar Fd3m cubic phase. *Phys Chem Chem Phys* **2011**, *13* (8), 3033-8.